Supplementary Material

Enhanced Removal of Sulfonamide Antibiotics by Spent Coffee Ground-Derived Biochars Produced Under a CO_2 Atmosphere

Wenting Li, Xian Yuan, Binrong Li and Xiaofang Shen *

School of Environmental Science and Engineering, Suzhou University of Science and Technology, Suzhou 215009, China; liwenting2020@outlook.com (W.L.); yuanxian1004@outlook.com (X.Y.); libr@usts.edu.cn (B.L.)

* Correspondence: xiaofang@mail.usts.edu.cn; Tel.: +86-0512-68092481

Text S1 Detailed instrument information and measurement parameters for characterizations

The surface morphology of the biochars was observed using scanning electron microscopy (SEM, Quanta FEG 250, FEI, Hillsboro, OR, USA). The biochar was attached to the sample stage with conductive adhesive, coated with gold, and then observed under the SEM at an accelerating voltage of 10 kV and a magnification of 4000x.

The SSA and pore structure were characterized using a surface area and porosity analyzer (TriStar II Plus 3030, Micromeritics, Norcross, GA, USA). The biochar was degassed at 200°C for 8 hours. After degassing, N_2 adsorption–desorption experiments were conducted at 77 K using liquid nitrogen. SSA was calculated via the Brunauer–Emmett–Teller (BET) model, while the pore size distribution was determined using the Barrett–Joyner–Halenda (BJH) and Microporosity analysis methods.

Thermogravimetric (TG) and derivative thermogravimetric (DTG) curves of the SCG were acquired using a simultaneous thermal analyzer (STA 449 F3, Netzsch–Gerätebau GmbH, Selb, Germany) by heating the samples to 900°C at a rate of 5°C·min^{-1} under either CO_2 or Ar atmospheres (where Ar was used to simulate the oxygen-limited environment [83]).

The water contact angle (WCA) on the biochar surface was measured via the sessile drop method (5 μL ultrapure water) using a contact angle meter (Model 500, Rame-hart Instrument Co., Succasunna, NJ, USA). Each sample was measured in triplicate, and the average value was reported.

Fourier-transform infrared spectrometry (FTIR, Nicolet 6700, Thermo Fisher Scientific, Waltham, MA, USA) was applied to compare the differences in surface functional groups of biochars. The biochars and KBr were dried at 60°C for 12 hours, and then mixed at a 1:100 (w:w) ratio in an agate mortar. After that, the mixed samples were pressed into tablets for testing. The scanning wavenumber range is 400–4000 cm^{-1}.

The degree of graphitization was evaluated using a micro-laser Raman spectrometer (DXR microscope, Thermo Fisher Scientific, Waltham, MA, USA) [60] with a 532 nm laser. Spectra were recorded from 100 to 3500 cm^{-1}, and the I_D/I_G intensity ratio (D band ~1350 cm^{-1}, G band ~1590 cm^{-1}) was used to evaluate the graphitization degree.

The surface elemental compositions (C, N, and O) and their chemical states were determined via X-ray photoelectron spectroscopy (XPS, Thermo Scientific K-Alpha, Thermo Fisher Scientific, Waltham, MA, USA). The spot size is 400 μm, with an operating voltage of 12 kV and a filament current of 6 mA. For full-spectrum scanning, a pass energy of 150 eV with a step size of 1 eV was applied; for narrow-spectrum scanning, a pass energy of 50 eV with a step size of 0.1 eV was applied. When performing XPS peak fitting, C1*s* of 284.80 eV was set as the energy standard for charge correction.

The zeta potential of the biochars was measured using a Zetasizer Nano ZS (Malvern Instruments Ltd., Malvern, UK). Before testing, the biochar samples were mixed with deionized water and the solution pH was adjusted to between 1.0, 3.0, 5.0, 7.0, 9.0, and 11.0.

The ash content was determined according to the slow ashing method specified in GB/T 212-2008 (Proximate Analysis of Coal) [84], which is technically equivalent to ISO 1171 (Solid mineral fuels—Determination of ash). Briefly, approximately 1 g of biochar was evenly spread in a pre-ignited ash crucible of constant mass, with a loading no greater than 0.15 g cm^{-2}. The crucible was placed in the uniform-temperature zone of a muffle furnace preheated to no more than 100°C, with the furnace door closed but left with a gap of approximately 15 mm. The temperature was then raised slowly to 500°C over a period of no less than 30 min and maintained at 500°C for 30 min. Subsequently, the temperature was increased to 815±10°C and the sample was ignited at this temperature for 1 h, followed by check-ignitions to constant mass. The ash content was calculated as the mass percentage of the residue.

Text S2 Method of Density functional theory calculations

Density functional theory (DFT) calculations were performed using the Vienna Ab-initio Simulation Package (VASP) to investigate the interaction mechanisms between sulfonamide antibiotics (SAs) and nitrogen-containing carbon structures [85]. The projector-augmented wave (PAW) method was employed [86]. The exchange correlation energy was calculated using the Perdew–Burke–Ernzerhof (PBE) functional [87] with Grimme's DFT-D3 dispersion correction [88]. The carbon surface models containing pyrrolic-N and pyridinic-N configurations were constructed to represent the dominant nitrogen-containing active sites in biochar. A vacuum layer of 30 Å was introduced along the z-direction to eliminate artificial interactions between periodic images. The plane-wave cutoff energy was set to 520 eV. The Brillouin zone was sampled using Gamma-centered k-

point meshes of 1 × 1 × 1 [89]. All structures were fully optimized until the energy convergence criterion reached 10^{-5} eV and the residual forces on each atom were below 0.02 eV $Å^{-1}$. The electrostatic potential (ESP) distributions of SA molecules were calculated based on the optimized structures to identify electron-rich and electron-deficient regions involved in intermolecular interactions.

The adsorption energies (E_{ads}) were calculated according to the following equation:

$$E_{ads} = E_{SAs/substrate} - E_{SAs} - E_{substrate}$$

where $E_{SAs/substrate}$, E_{SAs}, and $E_{substrate}$ represent the total energies of the optimized adsorption complex, isolated SA molecule, and isolated carbon substrate, respectively. A more negative adsorption energy indicates a stronger interaction between SA molecules and carbon surfaces.

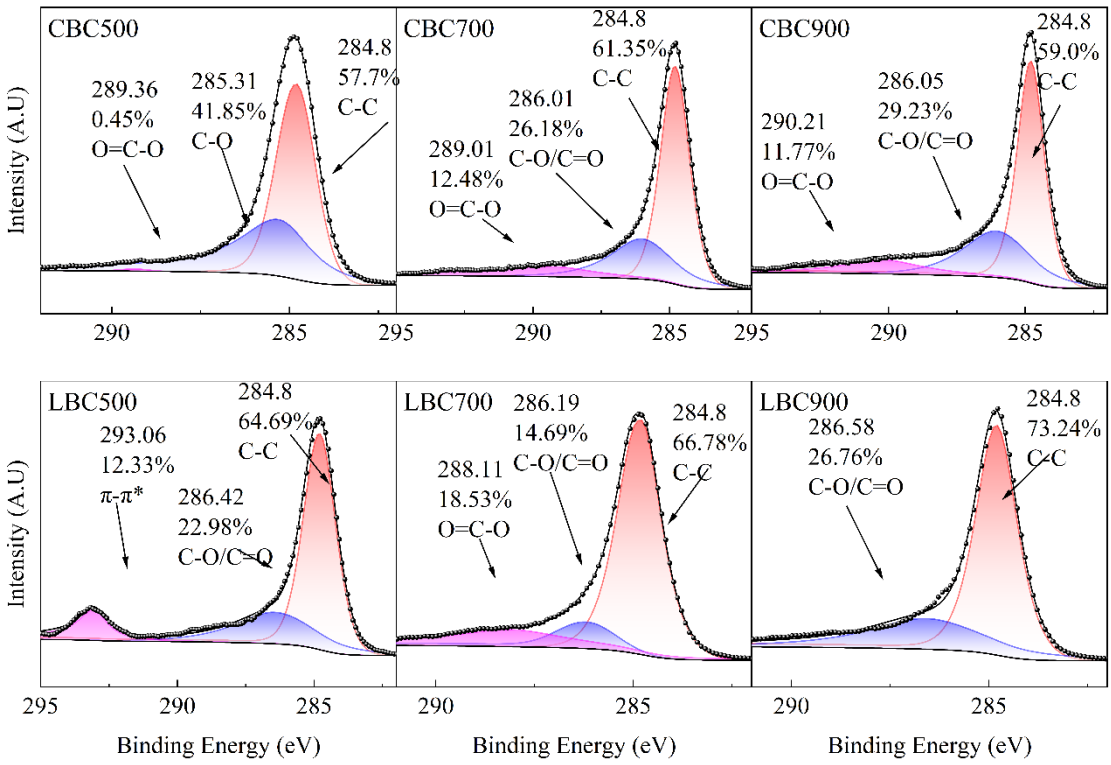

Figure S1. High-resolution C1*s* spectra of biochar.

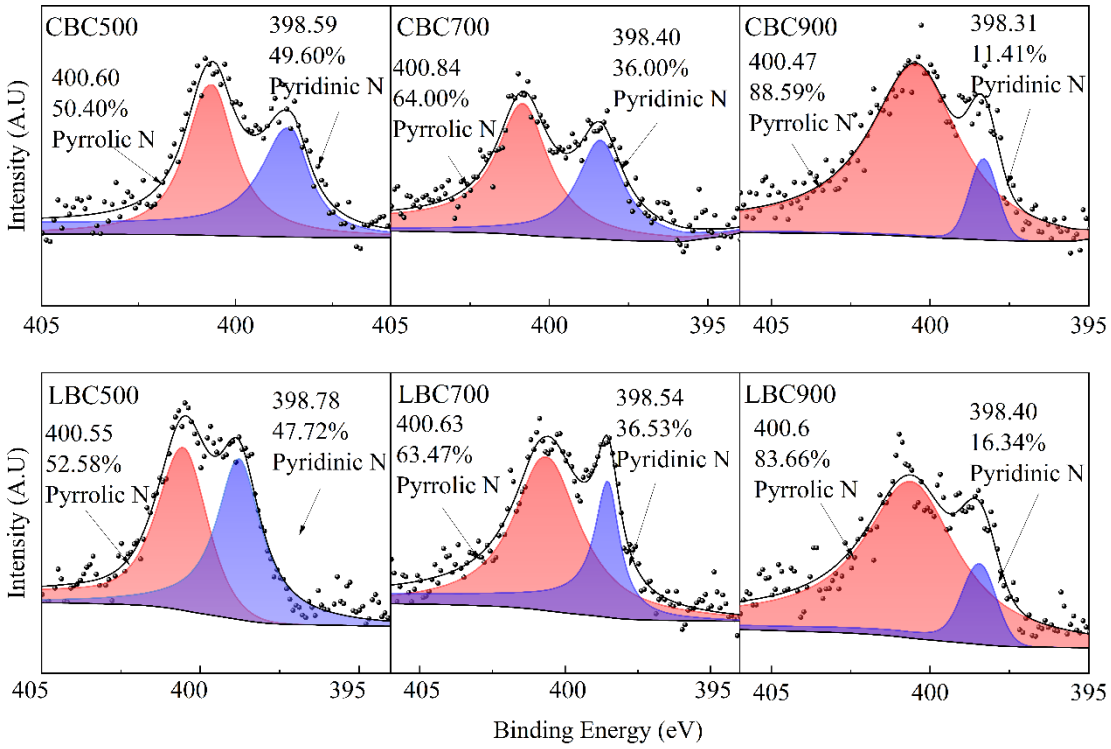

Figure S2. High-resolution N1*s* spectra of biochar.

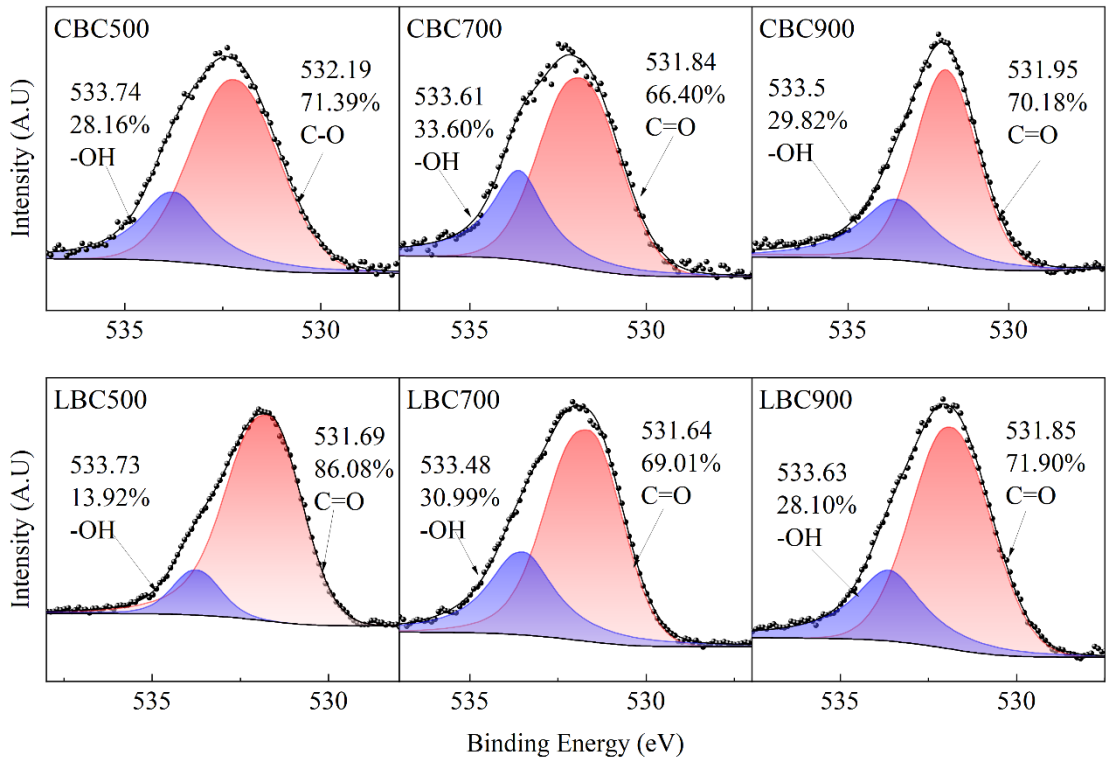

Figure S3. High-resolution O1*s* spectra of biochar.

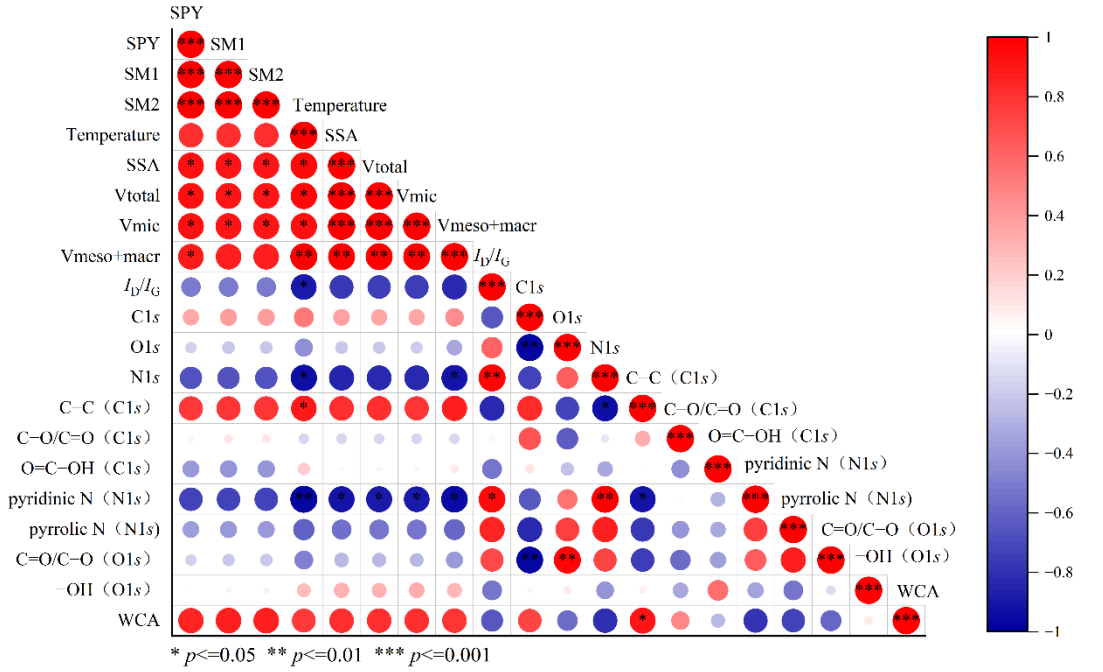

Figure S4. Correlation heatmap of biochar properties and SA adsorption capacity after excluding CBC900.

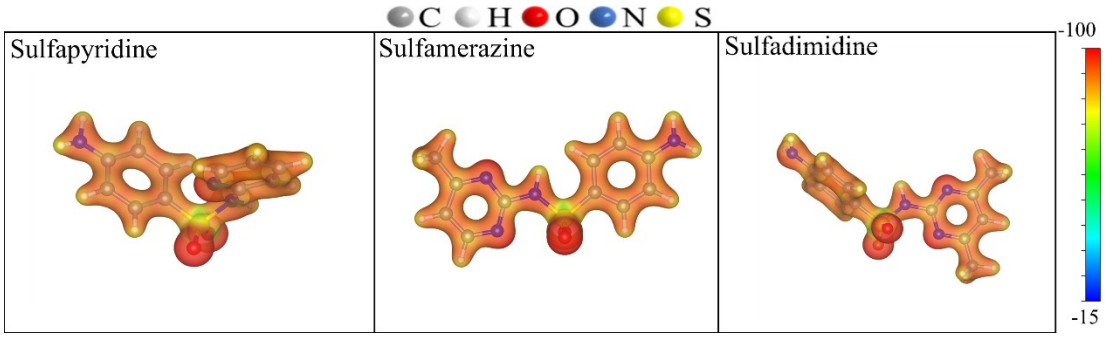

Figure S5. Electrostatic potentials of sulfapyridine, sulfamethazine, and sulfadimethoxine.

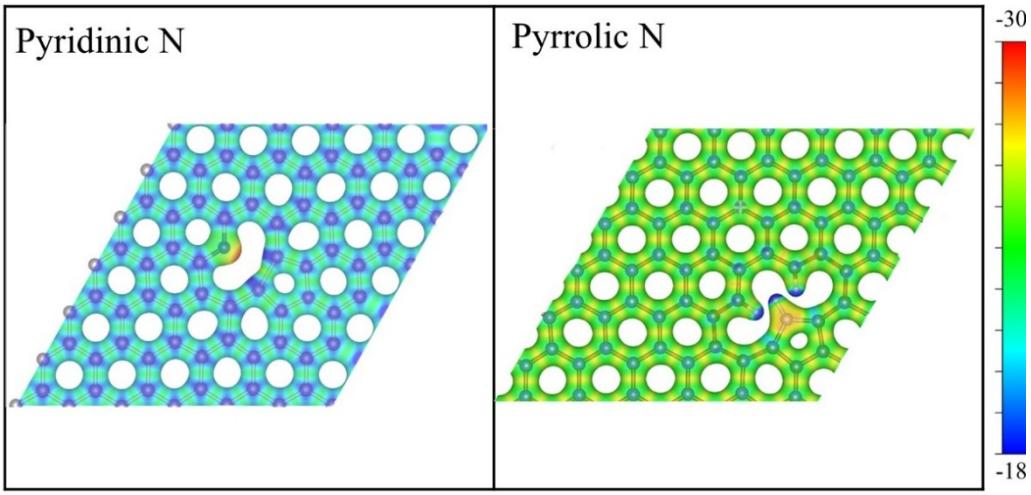

Figure S6. Electrostatic potential of simulated biochar within pyridinic N and pyrrolic N.

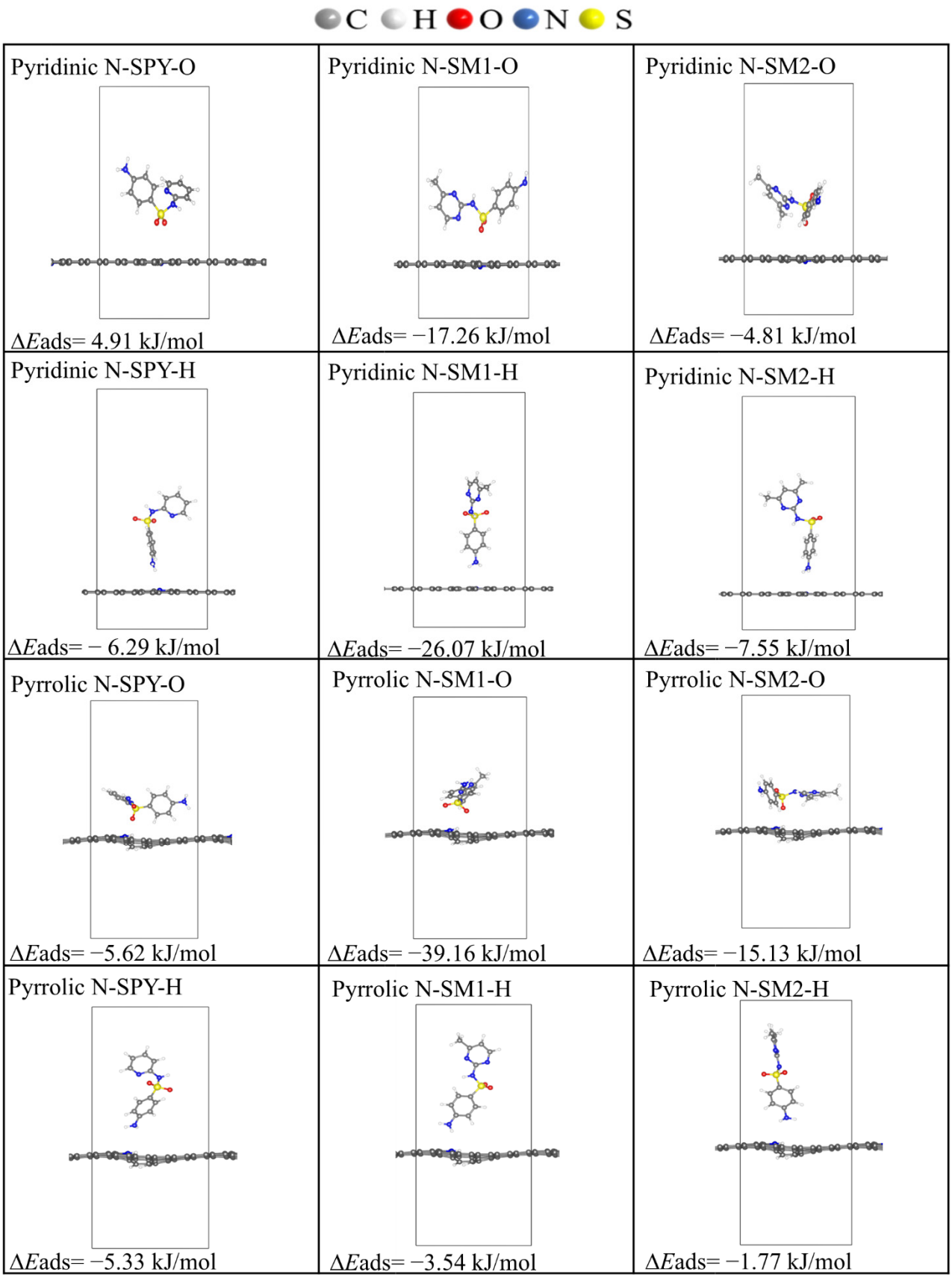

Figure S7. Adsorption of SAs by simulated biochar within pyridinic N and pyrrolic N.

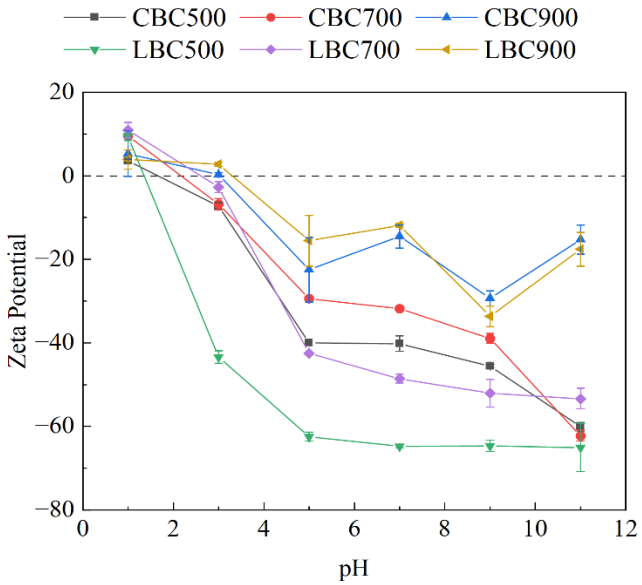

Figure S8. Zeta potentials of the raw biochars.

Table S1. Solid-to-liquid ratios applied in adsorption experiment.

SAs	CBC500 mg/5 mL	CBC700 mg/5 mL	CBC900 mg/100 mL	LBC500 mg/5 mL	LBC700 mg/5 mL	LBC900 mg/40 mL
SPY	47	35	1	11	5	1.5
SM1	58	25	1	90	10	1.2
SM2	70	34	1	60	15	2

Table S2. Specific surface area and pore structure parameters of the biochars.

Biochar	SSA[a] ($m^2 \cdot g^{-1}$)	V_{total}[b] ($cm^3 \cdot g^{-1}$)	V_{mic}[c] ($cm^3 \cdot g^{-1}$)	$V_{meso+macr}$[d] ($cm^3 \cdot g^{-1}$)	D_p[e] (nm)
CBC500	-	-	-	-	-
CBC700	77.88	0.04335	0.03137	0.01199	2.227
CBC800	400.3	0.2092	0.1946	0.01462	2.091
CBC900	1025	0.5583	0.3995	0.1588	2.178
LBC500	1.696	0.004050	-	-	-
LBC700	192.0	0.1002	0.08617	0.01399	2.087
LBC900	436.4	0.2269	0.1988	0.02804	2.077

[a] Specific surface area; [b] V_{total}, total pore volume; [c] micropore volume with pore size < 2 nm; [d] meso- and macropore volume with pore sizes of 2-50 nm and > 50 nm; [e] average pore diameter; "-" indicates not detected.

Table S3. Yields and ash contents of the biochar samples.

Biochar	Yield (%)	Biochar yields relative to CBC900	Ash content (%)
CBC500	27.69	1.90	2.72
CBC700	24.21	1.67	3.32
CBC900	14.54	1.00	5.73
LBC500	28.96	1.99	2.86
LBC700	24.84	1.71	3.20
LBC900	21.38	1.47	3.82

Table S4. Fitting parameters of adsorption isotherms for SAs onto the biochars.

Pollutants	Adsorbents	Langmuir model			Freundlich model		
		q_m (mg·g^{-1})	K_L (L·mg^{-1})	R^2	K_F (mg·g^{-1}/(mg·L^{-1})$^{1/n}$)	1/n	R^2
SPY	CBC500	0.2862	0.3687	0.967	0.0817	0.4966	0.993
	CBC700	0.2866	0.8472	0.986	0.1235	0.3799	0.977
	CBC900	262.7	2.485	0.871	164.7	0.2443	0.942
	LBC500	1.340	0.1116	0.983	0.1513	0.6990	0.984
	LBC700	2.574	0.5853	0.963	0.9403	0.4373	0.984
	LBC900	33.31	2.716	0.965	21.50	0.2211	0.906
SM1	CBC500	0.0884	0.3996	0.986	0.0265	0.4600	0.956
	CBC700	0.1882	0.8060	0.979	0.0837	0.3527	0.943
	CBC900	220.1	3.699	0.964	154.2	0.1858	0.841
	LBC500	0.0703	0.1906	0.992	0.0128	0.5864	0.992
	LBC700	0.5399	0.7700	0.983	0.2317	0.3580	0.936
	LBC900	30.42	0.4599	0.973	10.02	0.4327	0.972
SM2	CBC500	0.1123	0.6529	0.932	0.0463	0.3640	0.870
	CBC700	0.2297	2.089	0.793	0.1357	0.2698	0.914
	CBC900	244.5	0.6675	0.915	100.9	0.3754	0.961
	LBC500	0.1109	0.5172	0.977	0.0404	0.4025	0.947
	LBC700	0.4562	2.702	0.909	0.3049	0.2090	0.941
	LBC900	23.86	2.647	0.926	16.51	0.2369	0.961

Note: The Freundlich model yields better fitting for adsorption isotherm data, indicative of heterogeneous adsorption sites. However, K_F is an empirical parameter inherently coupled with 1/n and lacks a saturation limit. Thus, K_F is not used for quantitative comparison of adsorption capacity in this work and is provided only for supplementary reference.

Table S5. Adsorption performance comparison of raw biochars toward organic pollutants.

Biomass	Pyrolysis temperature (℃)	Pyrolysis atmosphere	Target pollutant	Langmuir q_{max} (mg/g)	Ref.
Spent coffee grounds	800	N_2	Carbamazepine	31.40	[90]
Spent coffee grounds	500	Limited oxygen	Sulfadiazine	0.2219	[29]
Spent coffee grounds	400	Limited oxygen	Sulfamethoxazole	0.4816	[29]
Spent coffee grounds	500	N_2	Tetracycline	39.22	[91]
Spent coffee grounds	550	N_2	Diclofenac	61.17	[92]
Spent coffee grounds	550	N_2	Levofloxacin	110.70	[92]
Spent coffee grounds	500	N_2	Tetracycline	95.34	[93]
Cattle manure	900	CO_2	Sulfamethoxazole	41.20	[94]
Cattle manure	900	N_2	Sulfamethoxazole	28.92	[94]
Enteromorpha prolifera	800	N_2	Sulfamethoxazole	29.91	[95]
Bamboo	450	N_2	Sulfapyridine	57.90	[96]
Spent coffee grounds	900	Limited oxygen	Sulfapyridine	33.31	This study
Spent coffee grounds	900	Limited oxygen	Sulfamerazine	30.42	This study
Spent coffee grounds	900	Limited oxygen	Sulfamethazine	23.86	This study
Spent coffee grounds	900	CO_2	Sulfapyridine	262.7	This study
Spent coffee grounds	900	CO_2	Sulfamerazine	220.1	This study
Spent coffee grounds	900	CO_2	Sulfamethazine	244.5	This study

Note: In [92] and [93], coffee grounds are activated with phosphoric acid.

Table S6. Pearson correlation coefficients (r) and p-values between key physicochemical parameters and Langmuir maximum adsorption capacity (Q_m) of SPY, SM1 and SM2.

Parameter	Sample	Index	SPY-Q_m	SM1-Q_m	SM2-Q_m
SSA	All sample	r	0.9509	0.9639	0.9429
		p	0.0036	0.0032	0.0048
SSA	Excluding CBC900	r	0.9218	0.9092	0.9090
		p	0.0257	0.0324	0.0325
V_{total}	All sample	r	0.9563	0.9591	0.9487
		p	0.0028	0.0025	0.0039
V_{total}	Excluding CBC900	r	0.9262	0.9134	0.9132
		p	0.0238	0.0302	0.0303
V_{mic}	All sample	r	0.9239	0.9277	0.9140
		p	0.0085	0.0077	0.0108
V_{mic}	Excluding CBC900	r	0.9201	0.9063	0.9061
		p	0.0268	0.0339	0.0341
$V_{meso+macr}$	All sample	r	0.9958	0.9960	0.9943
		p	2.630×10^{-5}	2.398×10^{-5}	4.793×10^{-5}
$V_{meso+macr}$	Excluding CBC900	r	0.8821	0.8732	0.8733
		p	0.0477	0.0531	0.0531
I_D/I_G ratio	All sample	r	−0.5255	−0.5307	−0.5147
		p	0.2843	0.2786	0.2962
I_D/I_G ratio	Excluding CBC900	r	−0.5120	−0.5098	−0.5099
		p	0.3778	0.3802	0.3801
Pyrrolic-N	All sample	r	0.9173	0.9132	0.9231
		p	0.0099	0.0110	0.0087
Pyrrolic-N	Excluding CBC900	r	−0.3698	−0.3832	−0.3830
		p	0.5401	0.5244	0.5246

Table S7. Physicochemical properties of the three SAs.

Pollutants	**Molecular formula**	**logK_{ow}**	**pK_{a1}**	**pK_{a2}**
SPY [97]	$C_{11}H_{11}N_3O_2S$	0.35	2.3	8.4
SM1 [68]	$C_{11}H_{12}N_4O_2S$	0.11	2.16	6.8
SM2 [68]	$C_{12}H_{14}N_4O_2S$	0.27	2.46	7.45

References:

29. Zhang, X.; Zhang, Y.; Ngo, H. H.; Guo, W.; Wen, H.; Zhang, D. et al. Characterization and sulfonamide antibiotics adsorption capacity of spent coffee grounds based biochar and hydrochar. *Sci. Total Environ.* **2020**, 716, 137015.
60. Li, X.; Cen, K.; Li, J.; Jia, D.; Gao, J.; Zhang, L. et al. Insights into the interactions between cellulose and hemicellulose during pyrolysis for optimizing the properties of biochar as a potential energy vector. *Ind. Crops Prod.* **2025**, 223, 120126.
68. Chen, Z.; Xiao, X.; Xing, B.; Chen, B. pH-dependent sorption of sulfonamide antibiotics onto biochars: Sorption mechanisms and modeling. *Environ. Pollut.* **2019***,* 248, 48–56.
83. Guo, J.; Zheng, L.; Li, Z.; Zhou, X.; Cheng, S.; Zhang, L. et al. Effects of various pyrolysis conditions and feedstock compositions on the physicochemical characteristics of cow manure-derived biochar. *J. Clean. Prod* **2021***,* 311, 127458.
84. GB/T 212-2008. Proximate analysis of coal. China Standards Press: Beijing, China, **2008**.
85. Hafner, J. Ab-initiosimulations of materials using VASP: Density-functional theory and beyond. *J. Comput. Chem.* **2008**, 29, 2044–2078.86.
86. Blöchl, P. E. Projector augmented-wave method. *Phys. Rev. B* **1994**, 50, 17953–17979.
87. Perdew, J. P.; Burke, K.; Ernzerhof, M. Generalized gradient approximation made simple. *Phys. Rev. Lett.* **1996**, 77, 3865–3868.
88. Grimme, S. Semiempirical GGA-type density functional constructed with a long-range dispersion correction. *J. Comput. Chem.* **2006**, 27, 1787–1799.
89. Monkhorst, H. J.; Pack, J. D. Special points for Brillouin-zone integrations. *Phys. Rev. B* **1976**, 13, 5188–5192.
90. Kwon, Y.; Kim, S.; Moon, S.; Yum, J.; Shin, J.; Kwak, J. et al. Enhanced adsorption of pharmaceuticals using coffee ground biochars via $KHCO_3$ and urea pre-treatment: Effects of π-π interactions and hydrogen bonding. *Environ. Chem. Ecotoxicol.* **2027**, 9, 92–103.
91. Nguyen, V.-T.; Nguyen, T.-B.; Huang, C. P.; Chen, C.-W.; Bui, X.-T.; Dong, C.-D. Alkaline modified biochar derived from spent coffee ground for removal of tetracycline from aqueous solutions. *J. Water Process Eng* **2021***,* 40, 101908.
92. Maged, A.; Dissanayake, P. D.; Yang, X.; Pathirannahalage, C.; Bhatnagar, A.; Ok, Y. S. New mechanistic insight into rapid adsorption of pharmaceuticals from water utilizing activated biochar. *Environ. Res.* **2021**, 202, 111693.
93. Huyen, V. L. D.; Nguyen, T. H.; Truong-Lam, H. S. Phosphoric-acid-activated biochar derived from spent coffee grounds as sustainable adsorbent for solid-phase extraction. *Mater. Today Commun.* **2026***,* 54, 115590.
94. Yoon, K.; Kwon, G.; Kim, E.; Lee, H.; Lee, D.-J.; Song, H. Pyrolytic conversion of cattle manure into value-added products and application of biochar for adsorption of sulfamethoxazole. *Chemosphere* **2024***,* 366, 143493.
95. Lin, S.; Shen, Z.; Pan, D.; Ji, R.; Bian, Y.; Han, J. et al. Marine macroalgae-derived multielement-doped porous biochars for efficient removal of sulfamethoxazole from aqueous solution: Sorption performance and governing mechanisms. *J. Anal. Appl. Pyrolysis* **2023***,* 171, 105963.
96. Huang, J.; Zimmerman, A. R.; Chen, H.; Gao, B. Ball milled biochar effectively removes sulfamethoxazole and sulfapyridine antibiotics from water and wastewater. *Environ. Pollut.* **2020***,* 258, 113809.
97. Huang, J.; Zimmerman, A. R.; Chen, H.; Wan, Y.; Zheng, Y.; Yang, Y. et al. Fixed bed column performance of Al-modified biochar for the removal of sulfamethoxazole and sulfapyridine antibiotics from wastewater. *Chemosphere* **2022***,* 305, 135475.